Plastic response of a two-dimensional amorphous solid to quasistatic shear: Transverse particle diffusion and phenomenology of dissipative events

Anaël Lemaître[1] and Christiane Caroli[2]
[1]*Institut Navier–LMSGC, CNRS–UMR 113, 2 allée Képler, 77420 Champs-sur-Marne, France*
[2]*INSP, Université Pierre et Marie Curie-Paris 6, CNRS, UMR 7588, 140 rue de Lourmel, 75015 Paris, France*
(Received 4 April 2007; revised manuscript received 21 May 2007; published 10 September 2007)

We perform extensive simulations of a two-dimensional Lennard-Jones glass subjected to quasistatic shear deformation at $T=0$. We analyze the distribution of nonaffine displacements in terms of contributions of plastic, irreversible events, and elastic, reversible motions. From this, we extract information about correlations between plastic events and about the elastic nonaffine noise. Moreover, we find that nonaffine motion is essentially diffusive, with a clearly size-dependent diffusion constant. These results, supplemented by close inspection of the evolving patterns of the nonaffine tangent displacement field, lead us to propose a phenomenology of plasticity in such amorphous media. It can be schematized in terms of elastic loading and irreversible flips of small, randomly located shear transformation zones, elastically coupled via their quadrupolar fields.

DOI: 10.1103/PhysRevE.76.036104 PACS number(s): 62.20.Fe, 62.25.+g, 66.30.−h

I. INTRODUCTION

Plastic deformation of amorphous solids and, more generally, of jammed disordered media (foams, confined granular media, colloidal glasses,…) has been intensively studied in the past two decades. General agreement is now gradually emerging about the nature of the elementary dissipative events in these highly multistable systems. They consist of sudden rearrangements of small clusters comprising a few basic structural units, such as T_1 events in dry foams. In the case of glasses, where they cannot be observed directly, progress has come, following the pioneer work of Argon and collaborators, from extensive numerical studies [1–3]. More recently, simulations performed on model systems—Lennard-Jones (LJ) glasses—have proved very helpful to improve our understanding of the effect of topological disorder on the elastic as well as plastic shear response of amorphous solids.

MD simulations are instrumental in elucidating the thermal dependence of the flow stress $\sigma(\dot{\gamma})$ in the high strain rate ($\dot{\gamma} \gg 1$) regime. However, such conditions (finite T, high $\dot{\gamma}$) "blur" the microscopic motion, making it difficult to characterize precisely the elementary events, which are the building blocks on which constitutive laws should be based. For this purpose, a second class of numerical works have focused on the athermal ($T=0$), quasistatic ($\dot{\gamma} \to 0$) regime. In this later regime, hereafter abbreviated as AQS, when a sample is sheared at constant rate, the stress-strain $\sigma(\gamma)$ curve exhibits (see Fig. 1) elastic branches interrupted by discontinuous drops $\Delta\sigma$, which are the signature of the dissipative events. Beyond an initial transient, $\sigma(\gamma)$ fluctuates about an average value $\bar{\sigma}$, which is identified with the yield stress $\sigma_Y = \lim_{\dot{\gamma}\to 0} \bar{\sigma}(\dot{\gamma})$. The distribution of stress drops is broad and system-size dependent. In their study on a 2D LJ glass, Maloney and Lemaître [4] were able to analyze them in terms of cascades of elementary events, which we will term "flips." Each such flip involves both the strong rearrangement of a small cluster (~a few atoms), and the appearance of an associated quadrupolar elastic field. This result substantiates the representation of elementary processes as Eshelby-type [6] shear transformations [7].

However, it appears desirable to analyze AQS simulations in more detail, in order to shed light upon debated questions concerning phenomenologies based on the notion of shear transformation zones (STZ) [3,8,9]. Namely,

(1) Can the flipping clusters be associated with regions of the disordered solid, which retain their identity over a finite range of elastic loading before they reach their instability threshold?

(2) If so, do the simulations give information about the response of a zone to the elastic field generated by the flip of another zone?

(3) Can one evaluate the relative importance of the dynamic noise resulting from this mechanism as compared with disorder-induced fluctuations of the nonaffine elastic field?

In order to address these issues, we extend in this paper a recent study on a 2D LJ glass [10], by Tanguy *et al.*, which confirms that plastic flow is spatially heterogeneous. They claim that one should distinguish between two types of plastic events: strongly localized ones occurring during the initial loading phase ($\sigma \ll \sigma_Y$), and nonlocalized ones, which they term "nonpermanent shear bands." They also investigate

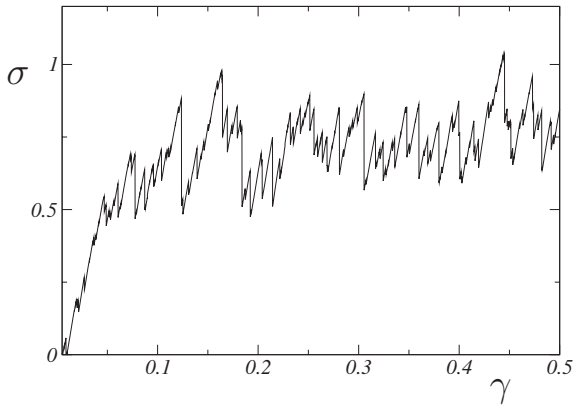

FIG. 1. Stress-strain curve for a 20×20 system.

atomic motion in the direction transverse to the plastic flow. While they find it to be diffusive at long times, they conclude to its hyperdiffusive nature on short time intervals.

Transverse displacements are purely nonaffine and, as indicated by the jagged shape of the $\sigma(\gamma)$ curve, consist of a succession of possibly noisy elastic episodes interspersed with sudden atomic rearrangements associated with the plastic events, hence the interest of a detailed analysis of their dynamics. With this remark in mind, we revisit in Sec. II the analysis of transverse particle motion, now explicitly separating elastic and plastic contributions. We thus extract information about (i) correlations between plastic events, and (ii) the elastic contribution to the nonaffine noise invoked in the phenomenological STZ model of Falk and Langer [9]. Moreover, we find it inappropriate to qualify global transverse particle motion as hyperdiffusive at short times. Indeed, the effective diffusion coefficient $D(\Delta\gamma)=\langle\Delta y^2\rangle/\Delta\gamma$ smoothly increases with $\Delta\gamma$ from a *finite* short time value D_0 to the asymptotic value D_∞. Noticeably, the whole $D(\Delta\gamma)$ curve is *system-size dependent*—a result which appears consistent with the analysis of plastic events in terms of flip cascades. We also show that the contribution of plastic events to transverse diffusion dominates markedly over the effect of disorder-induced nonaffine elastic fluctuations.

In Sec. III, on the basis of close inspection of the evolution of the spatial structure of the infinitesimal nonaffine field, we show that our results can be interpreted in terms of the elastic loading of zones driven by shear, which soften gradually as they approach their spinodal limit. As they approach this threshold, these zones give rise to quadrupolar fields of growing amplitude. The zones thus identified can be traced back over shear intervals substantially larger than the average interval between plastic events, the effect of which is thus easily observable.

These observations support a description in terms of elastically loaded zones, and point toward the relevance of the dynamical noise generated by plastic flips themselves. The associated interzone elastic couplings should be responsible for the "autocatalytic avalanches" [5,12] or flip cascades [4,13] constituting the system-size-dependent plastic events, which we believe to be precisely the nonpermanent shear bands invoked in Ref. [10]. We attribute the stronger localization of initial events to the smaller density of nearly unstable zones in the as-quenched or weakly stressed samples.

This empirical study thus leads to the emergence of a phenomenology of the nonaffine shear response summarized in Sec. IV. While supporting the concept of shear transformation zones (STZ) or, equivalently, elastically loaded traps (SGR), it diverges from these models about two of their basic assumptions, namely, independence of elementary events and the nature of noise. We think that it should be of use for further developments in the modelization of plasticity of amorphous media.

II. TRANSVERSE PARTICLE MOTION

A. 2D simulations in the AQS regime

We use here the same binary LJ mixture as that of Ref. [4], namely, large (L) and small (S) particle radii and numbers are $r_L=0.5$, $r_S=0.3$, and $N_L=N_S(1+\sqrt{5})/4$. These values ensure that no crystallization occurs at low temperature. Simple shear deformation is imposed using Lees-Edwards boundary conditions. We study systems of three different sizes $L\times L$, with $L=10,20,40$.

The quasistatic regime corresponds to the limit where the external time scale $\dot{\gamma}^{-1}$ is much larger than that of internal relaxation processes. The system, starting from local equilibrium, thus follows adiabatically the shear-induced evolution of the corresponding energy minimum up to the spinodal limit where this minimum disappears and the system jumps into another local minimum of lower energy. The simulation proceeds as follows: a small increment δ of homogeneous shear strain is imposed, then energy is minimized using a conjugate gradient algorithm with a stringent convergence criterion (see [4] for details). We choose $\delta=10^{-4}$, small enough to ensure that, for our system sizes, all elastic branches are well resolved. A typical $\sigma(\gamma)$ curve is displayed in Fig. 1.

Starting from an initial quench, we explore the shear range $\gamma\leq 2$. In order to characterize the stationary state, we only retain data for $\gamma>0.1$, which ensures that initial transients are discarded, thus making details of the quenching protocol immaterial. We have been able to collect data on 100, 50, and 20 systems of respective sizes $L=10,20,40$.

Following Ref. [4], we make extensive use of the so-called nonaffine tangent field $\{\mathbf{u_i}\}$, defined as the difference between the linear response of particle displacements to an increment of homogeneous strain and the corresponding homogeneous field. It is well defined, and is computed, everywhere along each elastic branch.

B. Statistics of transverse displacements

In plastically deforming amorphous systems, nonaffine displacement fields contain information about both, departures from standard continuum elastic behavior and the nature of plastic events. In our simple shear geometry, transverse particle displacements Δy_i are purely nonaffine, while longitudinal ones mix affine and nonaffine contributions. We thus focus on the normalized distributions $P(\Delta y,\Delta\gamma)$ of the Δy_i's for a fixed strain interval $\Delta\gamma$. The statistical ensemble is built by sampling, for all initial configurations, all the $\Delta y_i=y_i(\gamma_0+\Delta\gamma)-y_i(\gamma_0)$ at each step γ_0 $(0.1\leq\gamma_0\leq 2-\Delta\gamma)$.

Our results agree qualitatively with those of Tanguy *et al.* [10]. Namely (see Fig. 2), $P(\Delta y,\delta)$ has a quasi-Gaussian center and exhibits, beyond $\Delta y\sim 0.2$, an exponential tail. Its fine structure shows more clearly in the log-lin representation of the distribution $\tilde{P}(\zeta)$ of the scale variable $\zeta=\log_{10}(\Delta y)$. As displayed in Fig. 3, for small strain intervals ($\Delta\gamma/\delta\sim$a few units), the corresponding curves exhibit a peak at small Δy in the 10^{-4} range, together with a broad hump for larger values. As $\Delta\gamma$ increases, the peak shifts to the right and the hump amplitude grows, though without noticeable horizontal shift, until both merge, for $\Delta\gamma\approx 10^{-2}$.

Can we interpret this structure and its evolution in light of the succession of elastic and plastic episodes, which reflect into the sawtooth shape of the $\sigma(\gamma)$ response? Clearly, particle motion consists of a series of continuous trajectories

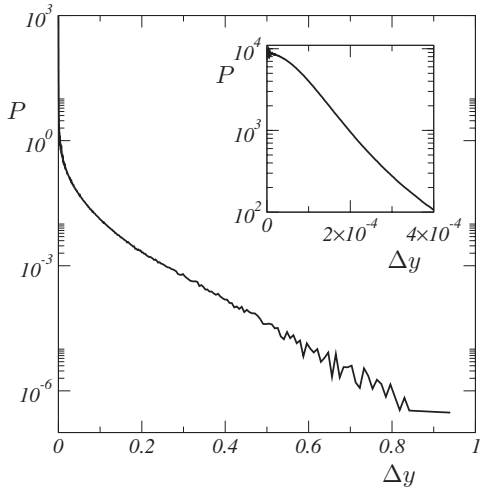

FIG. 2. The distribution $P(\Delta y, \delta)$ of transverse particle displacements for the elementary strain step δ and for system size $L=20$. Inset: Blow-up of the small Δy region.

interrupted by sudden jumps associated, respectively, with elastic episodes and plastic events. Since δ is our numerical strain resolution, each interval of length δ is, within our accuracy, defined as either purely elastic or purely plastic. So, for $\Delta\gamma=\delta$, we can decompose P (and likewise $\tilde{P}$) as

$$P(\Delta y,\delta)=\alpha_{pl}(\delta)\Pi_{pl}(\Delta y,\delta)+[1-\alpha_{pl}(\delta)]\Pi_{el}(\Delta y,\delta), \quad (1)$$

where $\alpha_{pl}(\delta)$ is the fraction of "plastic intervals" in our ensemble, and Π_{pl} (respectively, Π_{el}) are the normalized distributions associated with the plastic (respectively, elastic) subensemble. It now clearly appears (see Fig. 4) that the small Δy behavior of $P(\Delta y,\delta)$ results entirely from elastic motion, while its hump and large-Δy tail are due to plastic events.

On this basis, we are now able to understand the evolution of $\tilde{P}$ with $\Delta\gamma$. We extend the above decomposition to $\Delta\gamma$

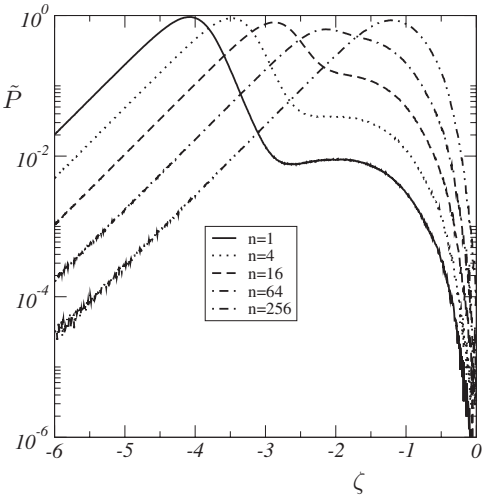

FIG. 3. The distribution $\tilde{P}(\zeta;\Delta\gamma)$ of the scale variable $\zeta=\log_{10}(\Delta y)$ for increasing values of $n=\Delta\gamma/\delta=1,4,16,64,256$. System size: $L=20$.

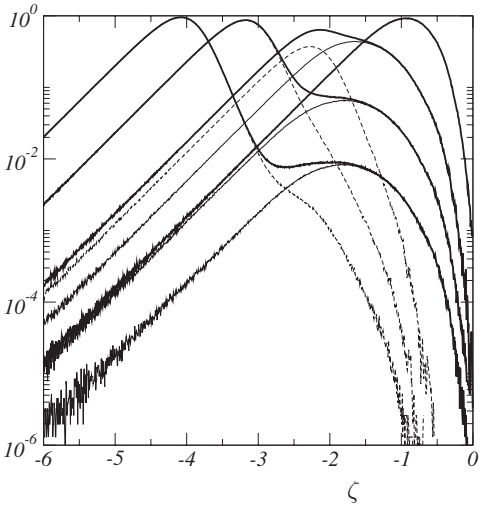

FIG. 4. Decomposition of the total distributions $\tilde{P}(\zeta;\Delta\gamma)$ (thick solid lines), for $n=\Delta\gamma/\delta=1,8,64,512$. For increasing n's, the maximum of the distribution shifts rightwards. Thin solid lines: contribution of plastic events; thin dashed lines: contribution of elastic branches (see text). System size $L=20$.

$>\delta$, now defining as "plastic" any interval containing at least one plastic event. As $\Delta\gamma$ increases while remaining small with respect to the average length $(\delta\alpha_{pl}(\delta)^{-1})$ of an elastic branch, most plastic intervals in general still contain only one plastic event, so that their fraction $\alpha_{pl}(\Delta\gamma)\approx(\Delta\gamma/\delta)\alpha_{pl}(\delta)$, while Π_{pl} remains quasi unchanged, because the scale of plastic slips is large compared with that of elastic ones. This explains the evolution (Fig. 4) of the plastic hump which, as $\Delta\gamma$ increases, consists primarily in an upward shift with little change in shape.

In this regime, which corresponds to $\Delta\gamma/\delta\ll\alpha_{pl}(\delta)^{-1}$ ($\sim$100 for the 20×20 system), the fraction $\alpha_{el}=(1-\alpha_{pl})$ of purely elastic intervals remains nearly constant (e.g., for $L=20$ and $\Delta\gamma=10\delta$, $\delta\alpha_{el}/\alpha_{el}\sim0.1$), so that the variations with $\Delta\gamma$ of the elastic part of $\tilde{P}$, $\tilde{P}_{el}=\alpha_{el}(\Delta\gamma)\tilde{\Pi}_{el}$, directly reveal those of $\tilde{\Pi}_{el}$. Inspection of the numerical data suggests (see also Fig. 4) that the rightward shifts of $\tilde{P}_{el}(\zeta)$ are roughly equal to $\log_{10}(\Delta\gamma)$. The plot (Fig. 5) of $\tilde{P}_{el}$ vs $\log_{10}(\Delta y/\Delta\gamma)$ shows that the collapse is indeed excellent in the low and middle ranges of $(\Delta y/\Delta\gamma)$ values, but fails in the large Δy tails.

This collapse means that *during the purely elastic episodes separating plastic events nonaffine displacements are essentially convective*: the γ derivative of the y_i field is nearly constant over most of an elastic episode. This amounts to stating that the tangent nonaffine field $\{\mathbf{u_i}\}$, although spatially disordered [11], remains quasiquenched. Now, we know from Ref. [14] that this cannot be true when the system comes close below a spinodal threshold γ_c. Indeed, in these near-critical regions, a gradually softening elastic mode develops, leading to a $(\gamma_c-\gamma)^{-1/2}$ divergence of $\{\mathbf{u_i}\}$. Clearly, it is the contribution of these near-critical softened configurations which explains the large-Δy tails of $\tilde{\Pi}_{el}$. The tail deflation (Fig. 5) results from the fact that, as the interval $\Delta\gamma$

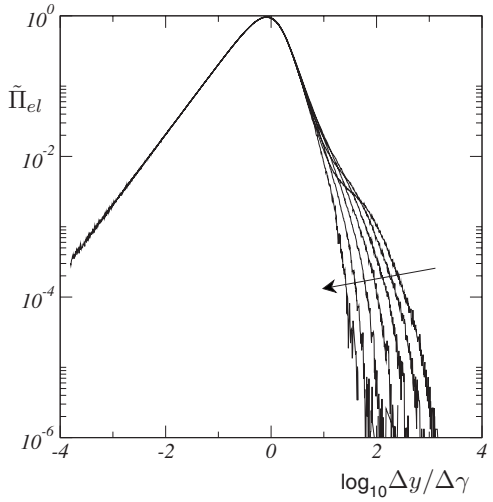

FIG. 5. The function $\tilde{\Pi}_{el}$ plotted vs $\log_{10}(\Delta y/\Delta\gamma)$ for $n=\Delta\gamma/\delta=1,2,4,8,16,32,64$. The arrow indicates the direction of *increasing* n's. System size $L=20$.

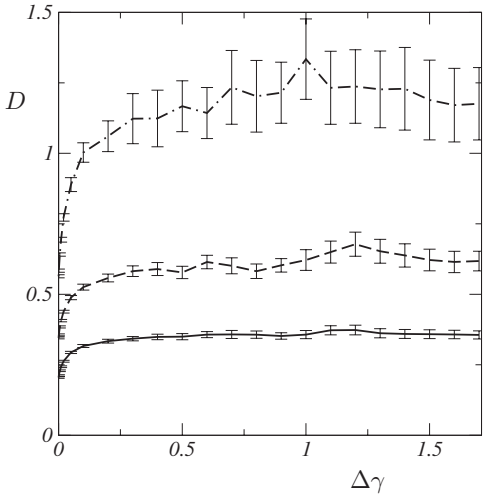

FIG. 6. From bottom to top: the instantaneous diffusion constant, $D(\Delta\gamma)=\langle\Delta y^2\rangle/\Delta\gamma$ vs $\Delta\gamma$, for increasing system sizes $L=10,20,40$ (and, respectively, 100, 50, and 20 samples). Error bars result from a standard student analysis of the data.

increases, the weight of these soft configurations is gradually transferred from $\tilde{\Pi}_{el}$ to $\tilde{\Pi}_{pl}$.

This analysis clarifies the physical significance of the shape of $P(\Delta y,\Delta\gamma)$ in the moderate $\Delta\gamma$ range (where its non-Gaussian parameter remains large [10]): (i) Its quasi-Gaussian center [11] results from small-scale nonaffine displacements accumulated along purely elastic segments, during which particle trajectories are essentially convected. (ii) Its quasiexponential tail arises from plastic jumps during plastic events.

For larger $\Delta\gamma/\delta \gtrsim \alpha_{pl}(\delta)^{-1}$, however, the decomposition of Eq. (1) loses physical content since the statistical weight of elastic intervals vanishes while $\tilde{\Pi}_{pl}$ mixes both elastic and plastic contributions. In order to circumvent this limitation, we concentrate in the following on the evolution with $\Delta\gamma$ of the second moment $\langle\Delta y^2\rangle$.

C. Transverse particle diffusion

In order to elucidate the nature of the transverse particle dynamics, we have computed from our data the space and ensemble average $\langle\Delta y^2\rangle$ for increasing values of $\Delta\gamma$. In Fig. 6 we plot the effective diffusion coefficient $D(\Delta\gamma)=\langle\Delta y^2\rangle/\Delta\gamma$. For our three system sizes, $D(\Delta\gamma)$ exhibits the same qualitative features, namely, it increases from a finite value $D_0=\lim_{\Delta\gamma\to 0} D$, and saturates at a finite value D_∞ for large $\Delta\gamma$ ($\gtrsim 0.5$). However, D is strikingly system-size dependent, $D^{(L)}(\Delta\gamma)$ increasing with L for all $\Delta\gamma$'s.

Again, in order to shed light on the origin of this behavior, let us separate explicitly the elastic and plastic contributions to nonaffine particle motion. Indeed, we can write

$$\frac{dy_i}{d\gamma} = u_{iy}(\gamma) + \sum_a Y_i^a \delta(\gamma-\gamma_a), \tag{2}$$

where a labels the strain values where irreversible events (avalanches) occur, so that

$$D(\Delta\gamma) = D_{ee}(\Delta\gamma) + D_{ep}(\Delta\gamma) + D_{pp}(\Delta\gamma), \tag{3}$$

with

$$D_{ee}(\Delta\gamma) = \frac{1}{\Delta\gamma}\left\langle \int_{\gamma_0}^{\gamma_0+\Delta\gamma} d\gamma \int_{\gamma_0}^{\gamma_0+\Delta\gamma} d\gamma' u_{iy}(\gamma)u_{iy}(\gamma') \right\rangle, \tag{4}$$

and D_{ep}, D_{pp} the corresponding cross-correlated and plastic-plastic contributions. These three functions carry the information about self- and cross-correlations of elastic and plastic nonaffine displacements.

Let us first consider the $\Delta\gamma\to 0$ limit. A straightforward asymptotic analysis taking into account the square-root divergence of the tangent field $\{\mathbf{u_i}(\gamma)\}$ at spinodal points leads to (see Fig. 7 for a numerical check)

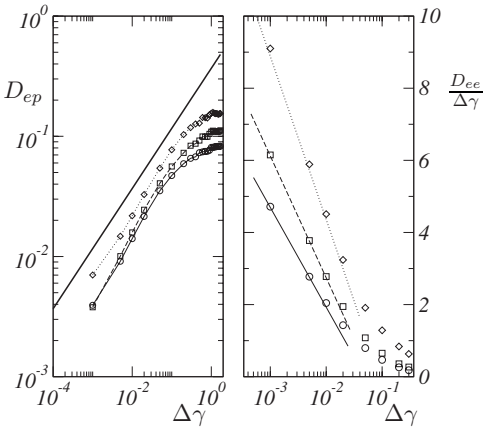

FIG. 7. Left: log-log plot of D_{ep} vs $\Delta\gamma$; the solid line has slope 1/2. Right: lin-log plot of $D_{ee}/\Delta\gamma$ vs $\Delta\gamma$; consistently with our analysis, the data asymptotes to straight lines at small $\Delta\gamma$ in this representation.

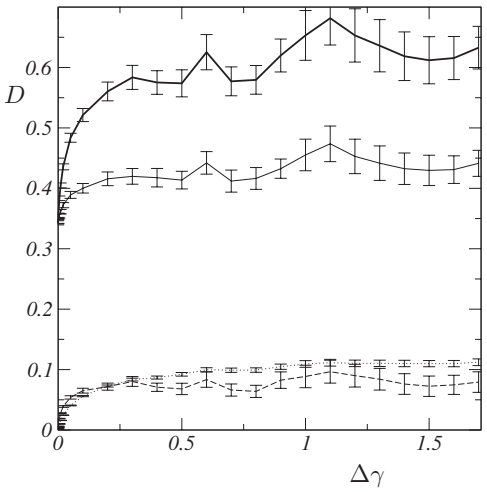

FIG. 8. The instantaneous diffusion constant $D(\Delta\gamma) = \langle \Delta y^2 \rangle / \Delta\gamma$ for system size $L=20$ (thick solid line) and its decomposition into D_{ee} (dotted line), D_{ep} (dashed line), and D_{pp} (thin solid line).

$$D_{ep}(\Delta\gamma) = O(\Delta\gamma^{1/2}), \tag{5}$$

$$D_{ee}(\Delta\gamma) = O(-\Delta\gamma \ln(\Delta\gamma)). \tag{6}$$

So, their contribution to $D(\Delta\gamma)$ vanishes, and the finite value of D_0 originates only from avalanches as follows:

$$D_0 = \lim_{\Delta\gamma \to 0} D_{pp} = f \langle (Y_i^a)^2 \rangle, \tag{7}$$

with

$$f = \lim_{\delta \to 0} \left[\frac{\alpha_{pl}(\delta)}{\delta} \right] \tag{8}$$

the average avalanche frequency, and $\langle (Y_i^a)^2 \rangle$ the variance of transverse displacements in a single plastic event.

It was shown in [4,13] that f increases with size roughly as the lateral system size L. Using the measured frequency, we find that the variance $\langle (Y_i^a)^2 \rangle = D_0 f^{-1}$ decreases slowly with size: for $L=10,20,40$, we get $10^4 \langle (Y_i^a)^2 \rangle = 37,26,20$. We will come back to this point later.

Figure 8 shows the decomposition [Eq. (3)] for $L=20$. It is seen that, for all, D_{pp} remains the dominant contribution. $D_{pp}(\Delta\gamma)$ grows, then saturates. Its growth range $\Gamma_{pp} \sim 0.25$ (see Fig. 9, bottom) shows no clear size dependence. This behavior entails that plastic events are correlated over a finite $\Delta\gamma$ range, which we understand as measuring a typical shear range over which the structural features involved in plastic events retain their identity.

For all sizes, $D_{ep}(\Delta\gamma)$, though much smaller than D_{pp}, exhibits an analogous behavior with a similar correlation range. This indicates that the above-mentioned persistent structures dominate the nonaffine elastic response. Moreover, the near square-root behavior [15] of D_{ep} for small $\Delta\gamma$ signals that the field $\{\mathbf{u_i}\}$ in a given near-critical region is strongly correlated with the displacements associated with the subsequent avalanche.

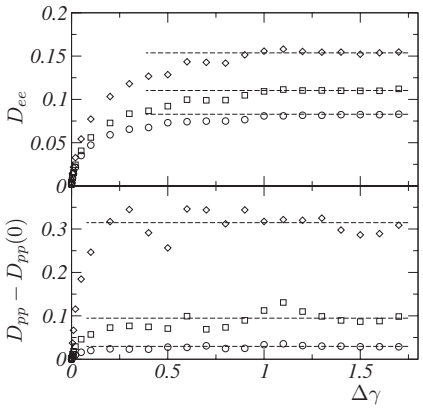

FIG. 9. $D_{ee}(\Delta\gamma)$ (top) and $D_{pp}(\Delta\gamma) - D_{pp}(0)$ (bottom) for system sizes, $L=10$ (circles), 20 (squares), and 40 (diamonds). The dashed lines indicate the asymptotic values of each of these data sets. For all system sizes, D_{pp} is seen to saturate after a strain interval $\Gamma_{pp} \sim 0.25$, while D_{ee} converges more slowly over $\Gamma_{ee} \sim 1$.

Finally, D_{ee} also rises and saturates, but more slowly than D_{ep} and D_{pp}. From the data for the three system sizes (Fig. 9, top), we evaluate its correlation range to be $\Gamma_{ee} \sim 1$. That is, a single renewal, after $\Delta\gamma \sim \Gamma_{pp}$, of the "active structures" is not sufficient for the nonaffine field to fully decorrelate. This we take as a hint of the fact that active structures occupy on average a fraction only of the total system "volume." With this interpretation, we evaluate this fraction as $\Gamma_{pp}/\Gamma_{ee} \sim 1/4$.

III. ZONE EMERGENCE, FLIPS, AND ELASTIC COUPLINGS

Two phenomenological models of plasticity of jammed disordered media—namely, the STZ theory of Falk and Langer [9,16], and the soft glass rheology (SGR) of Sollich *et al.* [17,18]—have been proposed recently. Both describe, explicitly (STZ) or implicitly (SGR), plastic events as transitions concerning small regions, modelized as either Eshelby-type transformations or jumps out of traps in the energy landscape. These flips are viewed as independent, hence individual, and governed by the combined effect of external drive and of a thermal-like noise.

A question then immediately arises: are our above results consistent with the basic ingredients of these models? We now try to answer it by careful inspection of the evolution of the spatial structure of the nonaffine tangent field $\{\mathbf{u_i}\}$.

A. Identification of active structures

Let us first recall that $\{\mathbf{u_i}\}$ can be written as [14]

$$u_{i\alpha} = H^{-1}_{i\alpha,j\beta} \Xi_{j\beta}, \tag{9}$$

$$\Xi_{j\beta} = -\frac{\partial^2 U}{\partial\gamma\, \partial r_{j\beta}}, \tag{10}$$

where (i,j) label particles and (α,β) label Cartesian components. U is the total energy of the LJ system, and $\bar{\bar{H}}$ is the

associated Hessian matrix. $\bar{\bar{\Xi}}\delta\gamma$ is the field of particle force increments generated by an infinitesimal increment of homogeneous shear. $\{\mathbf{u}=\mathbf{u_i}\}$ can be decomposed on the eigenmodes $\mathbf{\Psi_n}$ of $\bar{\bar{H}}$ (the phonon modes). Upon approaching a spinodal point, a single one, $\mathbf{\Psi}_1$, softens critically [14,19]. So, in near-critical regions, $\mathbf{u}$ exhibits a square-root divergence and is dominated by its projection $\mathbf{u}_1$ on $\mathbf{\Psi}_1$. This property enables us to clearly characterize the active structures close to the onset of plastic events.

The features we identify as characteristic of the evolution of $\mathbf{u}$ are exemplified in Figs. 8 and 9. In these figures, for each value of γ we decompose the total nonaffine field as

$$\mathbf{u} = \mathbf{u}_1 + \mathbf{u}_2 + \tilde{\mathbf{u}}, \tag{11}$$

with $\mathbf{u}_{1,2}$ its projections on the two modes $\mathbf{\Psi}_{1,2}$ with lowest eigenvalues $(\lambda_1 < \lambda_2)$.

We observe that, in all cases, the active structures emerge out of a quasirandom small background as one or several localized zones characterized by strong quadrupolar contributions to $\mathbf{u}$. These quadrupoles are approximately aligned with the principal directions of the homogeneous strain. As zones approach instability, they soften, and the corresponding growing part of $\mathbf{u}$ concentrates into the lowest mode component $\mathbf{u}_1$.

After identifying them in prespinodal regions, we are able to trace them *back* over sizeable γ ranges before their amplitude has decreased enough for them to gradually merge into the global disordered background structures. In some cases, this range of visibility extends across one or more plastic events. A typical sequence illustrating this behavior, shown on Fig. 10, extends over a range of $\Delta\gamma \sim 3\%$, to be compared with the average length $\Delta\gamma \sim 1\%$ of elastic episodes for this system size.

B. Zone flips

Each discontinuous drop on the $\sigma(\gamma)$ curve is associated with the sudden disappearance of one or more of these soft zones (Figs. 10 and 11). Noticeably, the resulting changes in $\{\mathbf{u_i}\}$ remain quite localized, leaving most of the other prominent structures of the nonaffine pattern essentially unchanged. In particular, zones which were already clearly visible are commonly seen to survive the plastic event (see Fig. 10).

We have shown in Sec. II B that particle jumps $\{\Delta\mathbf{R_i^a}\}$ in plastic events are well correlated with the precritical $\{\mathbf{u_i}\}$ structure. This entails that the flip of a zone Z is associated primarily with a quadrupolar displacement field of finite amplitude centered on Z. This supports the representation, proposed by Argon and co-workers [3,8] and explicated by Picard *et al.* [7], of the elementary dissipative process as the Eshelby-type shear transformation of a self-generated inclusion involving a few particles, which is also the basis of the STZ theory.

This representation is also consistent with the main features of the distribution $\Pi_{pl}(\Delta y, \delta)$ of particle displacements induced by plastic events (see Sec. II B). Indeed, the plot in Fig. 12 shows that Π_{pl} becomes exponential for $\Delta y \gtrsim 0.2$. In the Eshelby picture, we expect large Δy to correspond to displacements within the transforming zone(s), while smaller Δy are associated with particles sitting in the surrounding elastic medium. In this picture, we interpret the exponential tail of Π_{el}, hence of the full distribution P, as reflecting the diversity of intrazone structures. We thus expect that, upon varying the system size, the logarithmic slope of the tail should remain constant. As shown in Fig. 12, this prediction is very nicely verified for our three L values. Moreover, it appears that the tail amplitude decreases with increasing L. In our interpretation, the statistical weight of the exponential tail is controlled by the volume fraction of zone cores involved in plastic events. Since the average size of the avalanches constituting plastic events scales roughly as L, we expect the corresponding core volume fraction to decrease with size, in agreement with the observed behavior.

So, we interpret the existence of an exponential tail in $P(\Delta y)$ as a consequence of structural disorder within transforming zones, and by no means as a signature of avalanche behavior, which only affects the tail amplitude.

C. Elastic couplings

Consider the sequence shown in Fig. 11. For $\gamma=0.1150$ [Fig. 11(a)] two zones are clearly discernible in the $\mathbf{u}$ pattern. At $\gamma=0.1160$ [Fig. 11(b)] their amplitude has grown, and they appear in the projection $\mathbf{u}_2$ of $\mathbf{u}$ on the next-to-lowest mode. At $\gamma=0.1161$ [Fig. 11(c)] they are slightly softer and have invaded the projection $\mathbf{u}_1$ on the lowest mode. Note that, in these last two cases, they appear in the nontrivial soft mode as connected by "flow lines," which reproduce the most prominent vortex structures first described by Tanguy *et al.* [20]. This is particularly clear when two relatively distant zones soften simultaneously as shown in Fig. 13.

From these and many similar observations (see Fig. 10) we deduce that

(1) Soft zones are coupled elastically via their quadrupolar fields.

(2) It is the associated flow lines which form the conspicuous vortexlike patterns characteristic of nonaffine fields in amorphous solids. That such patterns are akin to incompressible flows results from the fact that these systems are much more compliant in shear than in compression. For our 2D LJ glass [4]: $\mu=39$, $K=236$.

Quadrupolar couplings result, in the homogeneous elastic continuum approximation for the background medium, from a stress field $\sim\cos(4\theta)/R^2$ (with R the length and θ the orientation with respect to $\hat{x}$ of the interzone vector). Notice that, in Fig. 11, in $\mathbf{u}_1$ the fields of the two zones Z_1,Z_2, which are quasivertically aligned, combine positively. We have checked that, in consistence with the above remark, zone pairs lying in sectors corresponding to negative couplings combine negatively in the phonons $\mathbf{\Psi}_1$ and $\mathbf{\Psi}_2$: in this case, one of the two zones appears with an opposite sign, i.e., with reversed flow lines. These observations confirm the relevance of interzone elastic couplings.

It is intuitively clear that configurations with strongly coupled soft zones are good candidates for simultaneous flips, as illustrated in Figs. 10 and 11. We observe a number

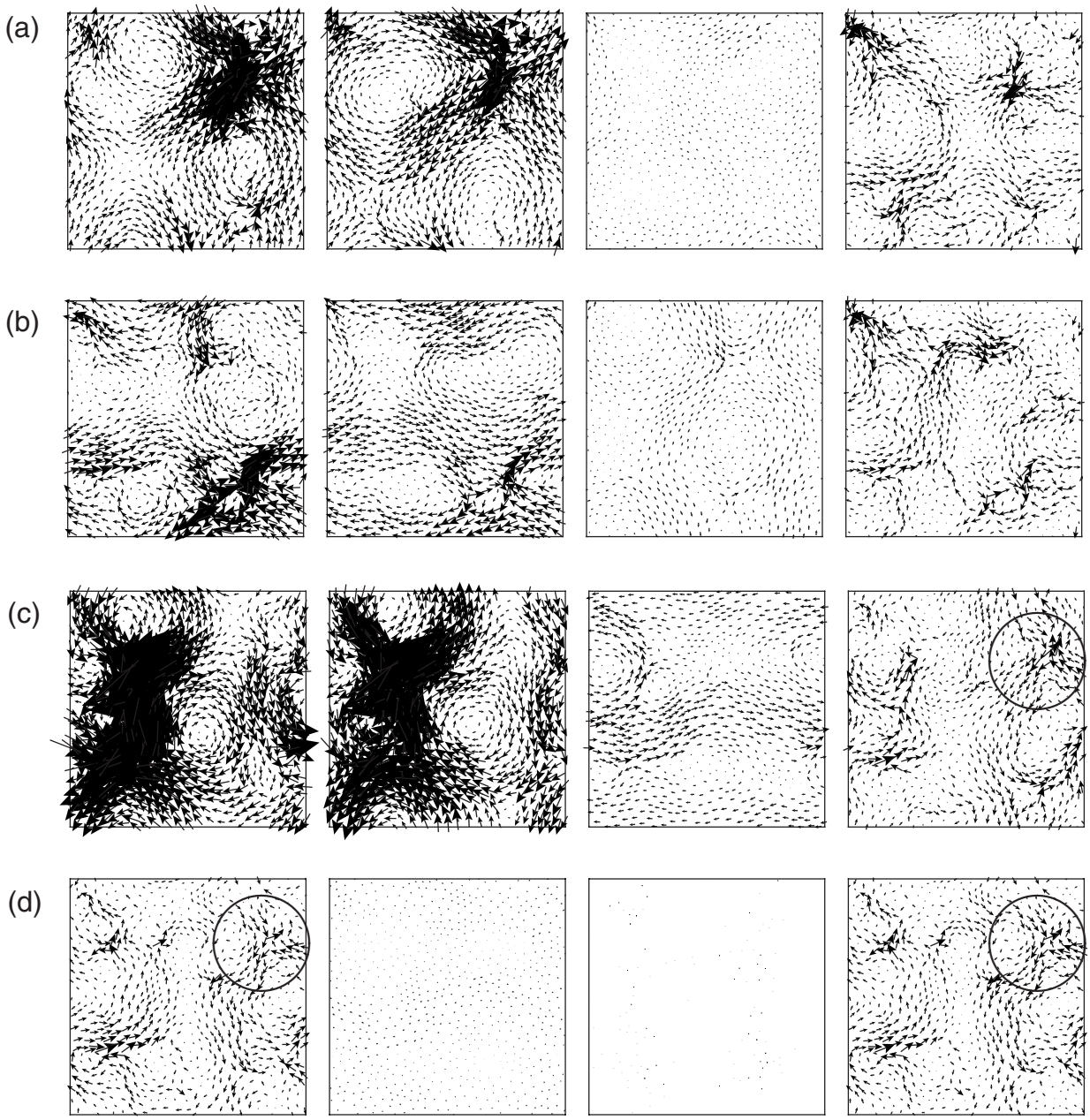

FIG. 10. System size: $L=20$. Each line corresponds to a single strain value γ. The four frames present, from left to right, the nonaffine tangent field $\mathbf{u}$ and its three components $\mathbf{u}_1$, $\mathbf{u}_2$, $\tilde{\mathbf{u}}$ as defined by Eq. (11). (a) $\gamma=0.0556$: a quadrupole, clearly visible in the upper right corner of both $\mathbf{u}$ and the soft mode component $\mathbf{u}_1$, signals a near-critical zone Z, which flips at $\gamma_c \in [0.0557, 0.0558]$. (b) $\gamma=0.0558$: Z has just flipped and disappeared, pushing another zone Z' (lowest right corners of $\mathbf{u}$ and $\mathbf{u}_1$) closer to its threshold. Note that Z' was already discernible (line a) in both $\mathbf{u}$ and $\tilde{\mathbf{u}}$ before the event. [(c) and (d)] Zone Z, now indicated by circles, can be traced *back* to $\gamma=0.0269$ (line c, frame $\tilde{\mathbf{u}}$). It survived the plastic event, which occurred in the interval 0.0269 (line c) and 0.0270 (line d).

of multizone flips, involving the disappearance of at least one diverging quadrupole, as well as that of some less visible zones. Moreover, plastic events alter the amplitude of the near-critical surviving zones in $\mathbf{u}$ (see Fig. 10) in a way which appears roughly consistent with quadrupolar couplings.

IV. PHENOMENOLOGY OF SHEAR ZONES

The various pieces of information, which we have gathered and presented above, can now be organized into a rather detailed phenomenology of plasticity in our system in the AQS regime, which can be schematized as follows.

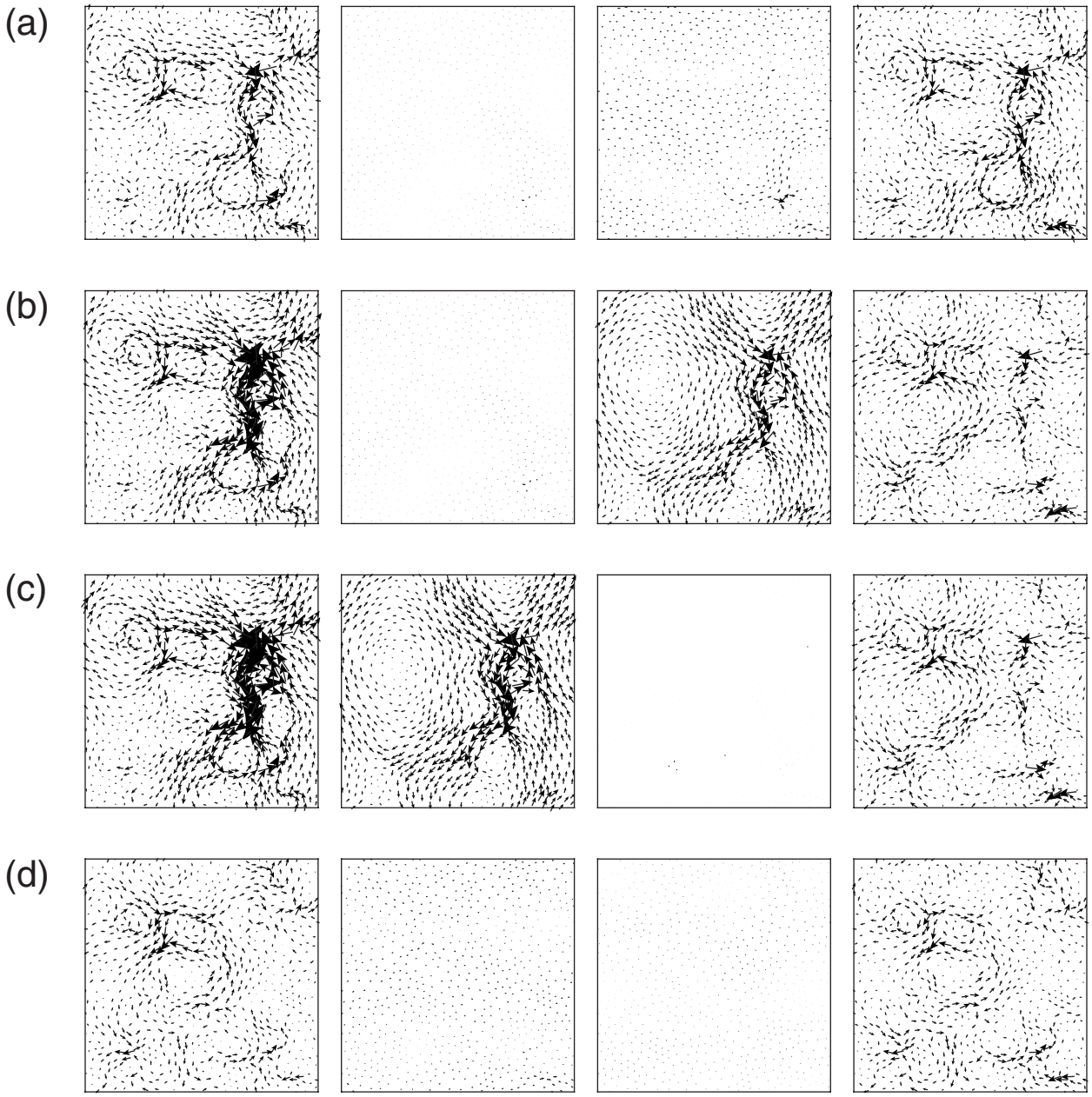

FIG. 11. From (a) to (d): γ=0.1150, 0.1160, 0.1161, and 0.1166. Two vertically aligned zones flip together in the interval 0.01165–0.01166 and disappear. As strain increases from γ=0.1150, they soften and sequentially appear in $\mathbf{u}_2$, then in $\mathbf{u}_1$ after a clear level crossing in the interval 0.01160–01161. The connecting flow lines are a signature of their elastic coupling.

(i) Structural disorder gives rise, in such a glassy system, to the existence of strong inhomogeneities, or zones. These zones can be viewed as small inclusions à la Eshelby, embedded in a quasihomogeneous elastic background, and plastically transformable under shear. They are advected by external shear toward their instability threshold. Upon approaching it, a zone softens, then flips at its spinodal and disappears.

The correlation range Γ_{pp} between plastic events (see Sec. II B) provides an evaluation of the amount of strain necessary to fully renew the population of zones. Here $\Gamma_{pp} \sim 0.25$.

One renewal is not sufficient, however, to decorrelate fully the nonaffine field. This suggests that zones occupy a fraction only of the system, of order Γ_{pp}/Γ_{ee}, here $\sim 1/4$.

(ii) Zone elastic softening and plastic flipping are both associated with quadrupolar components in the nonaffine displacement field, which give rise to interzone elastic couplings. Due to the long range of elastic fields, a zone flip thus alters the local strain level at any other zone site in the system, the resulting γ shift depending, in amplitude and sign, on the relative position of source and target. These signals have two types of effects.

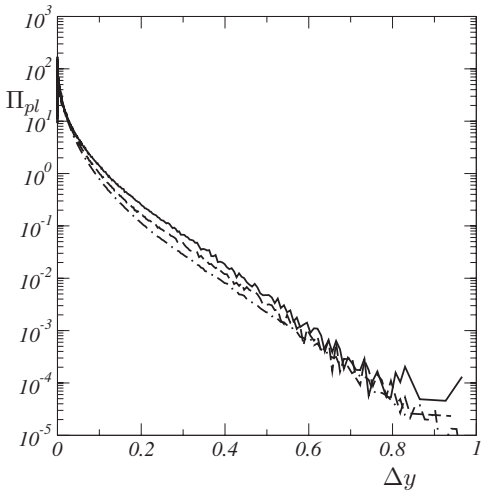

FIG. 12. The distribution $\Pi_{pl}(\Delta y, \delta)$ of particle displacements induced by plastic events for $L=10,20,40$.

(1) A flip signal may shift the strain level of some zones beyond their threshold γ_c, thus triggering their flip and initiating a cascade. In the quasi-state regime, where acoustic delays are neglected, such cascades are instantaneous.

(2) For the nonflipping zones, the elastic signals resulting from flips constitute a dynamical noise, acting in parallel with the externally imposed advection, whose frequency scale is proportional to the strain rate $\dot{\gamma}$.

So, in agreement with the previous proposition of Bulatov and Argon [3,8], also underlying recent models by Picard *et al.* [21] and by Baret *et al.* [22], we conclude that elastic couplings between zones play an essential role, by inducing avalanches and generating the dominant contribution to the disorder-induced noise. At $T=0$ and moderate strain rates, it is this dynamical elastic noise which, in addition to strain advection, must appear in models of plasticity of jammed media. In a forthcoming paper, we will propose such a schematic model, and show that it accounts for a system-size scaling behavior of avalanches.

Within the foregoing picture, we interpret the two kinds of events invoked by Tanguy *et al.* [10] as plastic events of different sizes. Namely, their transient shear bands exhibit the characteristics expected for large avalanches of the type described above, their directionality resulting from that of quadrupolar couplings in their system with two rigid walls. Their local events correspond to the small stress drops appearing during initial transients (see Fig. 1): at low stress levels, before advection has been able to significantly feed the near-threshold population, we indeed understand that avalanche triggering is unlikely, hence that single flip events are the rule.

Let us finally stress that the above zone phenomenology remains very schematic. Indeed, exhaustive inspection of the evolution of **u** reveals that zone life is somewhat more eventful than our simplified description suggests. Rather frequently, we see a given zone undergoing a few flips before it disappears. Such zones can be termed multistate. In other instances, a barely visible zone emerges fast enough to "overtake" previously more visible, softer, ones. That is, zone moduli and, very likely, thresholds are not unique, but distributed about an average. These remarks point toward the interest of pursuing extensive characterization of elastic heterogeneity in jammed systems, in particular, via studies of coarse grained elastic moduli.

On a more speculative level, we would like to raise an important question: are the irreversible transformations identified here under shear related to the dynamic heterogeneities [23–26] characteristic of glassy dynamics near and below T_g? Indeed, we share the opinion, formulated long ago by Goldstein [27], that at finite temperature "rearrangements are of course occurring all the time in the absence of an external stress; the external stress, by biasing them, reveals their existence".

Our active zones are primarily sensitive to shear. This, we think, must be put together with recent results by Widmer-Cooper and Harrowell [28,29]. These authors show that dynamic propensity in a 2D LJ glass is uncorrelated with free volume, which we understand to mean that their local rearranging structures are only weakly coupled to compression. This leads us to suggest that their observation that zones of high propensity have large "Debye-Waller factors" amounts to identifying them as soft zones sensitive to shear—a speculation which will demand extensive future investigation.

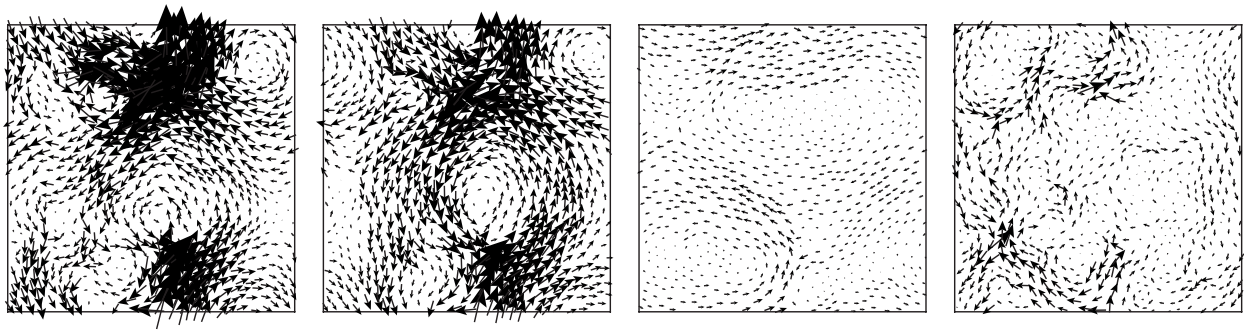

FIG. 13. Two distant zones soften simultaneously and appear in $\mathbf{u}_1$. The characteristic vortexlike structure signals their elastic coupling.

[1] S. Kobayashi, K. Maeda, and S. Takeuchi, Acta Metall. **28**, 1641 (1980).
[2] D. Deng, A. S. Argon, and S. Yip, Proc. R. Soc. London, Ser. A **329**, 549 (1989).
[3] A. S. Argon, V. V. Bulatov, P. H. Mott, and U. W. Suter, J. Rheol. **39**, 377 (1995).
[4] C. E. Maloney and A. Lemaître, Phys. Rev. E **74**, 016118 (2006).
[5] N. P. Bailey, J. Schiøtz, A. Lemaître, and K. W. Jacobsen, Phys. Rev. Lett. **98**, 095501 (2007).
[6] J. D. Eshelby, Proc. R. Soc. London, Ser. A **241**, 376 (1957).
[7] G. Picard, A. Ajdari, F. Lequeux, and L. Bocquet, Eur. Phys. J. E **15**, 371 (2004).
[8] V. V. Bulatov and A. S. Argon, Modell. Simul. Mater. Sci. Eng. **2**, 167 (1994).
[9] M. L. Falk and J. S. Langer, Phys. Rev. E **57**, 7192 (1998).
[10] A. Tanguy, F. Leonforte, and J.-L. Barrat, e-print arXiv:cond-mat/0605397.
[11] Note that the position of the peak of $\tilde{\Pi}_{el}$ corresponds, roughly, to the width of the Gaussian approximant of the small-Δy part of $P(y,\delta)$.
[12] M. J. Demkowicz and A. S. Argon, Phys. Rev. B **72**, 245206 (2005).
[13] C. Maloney and A. Lemaître, Phys. Rev. Lett. **93**, 016001 (2004).
[14] C. Maloney and A. Lemaître, Phys. Rev. Lett. **93**, 195501 (2004).
[15] Strictly speaking, in order to observe the asymptotic $\Delta\gamma^{1/2}$ behavior, we would need data for decreasing simulation strain intervals $\delta\to 0$. With our value $\delta=10^{-4}$, we measure at small $\Delta\gamma$ an effective behavior $D_{ep}\sim\Delta\gamma^{0.6}$.
[16] M. L. Falk and J. S. Langer, MRS Bull. **25**, 40 (2000).
[17] P. Sollich, F. Lequeux, P. Hébraud, and M. E. Cates, Phys. Rev. Lett. **78**, 2020 (1997).
[18] P. Sollich, Phys. Rev. E **58**, 738 (1998).
[19] D. L. Malandro and D. J. Lacks, J. Chem. Phys. **110**, 4593 (1999).
[20] A. Tanguy, J. P. Wittmer, F. Leonforte, and J.-L. Barrat, Phys. Rev. B **66**, 174205 (2002).
[21] G. Picard, A. Ajdari, F. Lequeux, and L. Bocquet, Phys. Rev. E **71**, 010501(R) (2005).
[22] J. C. Baret, D. Vandembroucq, and S. Roux, Phys. Rev. Lett. **89**, 195506 (2002).
[23] B. Doliwa and A. Heuer, Phys. Rev. E **67**, 031506 (2003).
[24] B. Doliwa and A. Heuer, Phys. Rev. E **67**, 030501(R) (2003).
[25] B. Doliwa and A. Heuer, Phys. Rev. Lett. **91**, 235501 (2003).
[26] T. B. Schrøder, S. Sastry, J. C. Dyre, and S. C. Glotzer, J. Chem. Phys. **112**, 9834 (2000).
[27] M. Goldstein, J. Chem. Phys. **51**, 3728 (1969).
[28] A. Widmer-Cooper and P. Harrowell, J. Phys.: Condens. Matter **17**, S4025 (2005).
[29] A. Widmer-Cooper and P. Harrowell, Phys. Rev. Lett. **96**, 185701 (2006).